Energy Conversion and Management 232 (2021) 113848

Contents lists available at ScienceDirect

Energy Conversion and Management

journal homepage: www.elsevier.com/locate/enconman

Environmentally-sound: An acoustic-driven heat pump based on phase change

Rui Yang [a], Nathan Blanc [b], Guy Z. Ramon [b,*]

[a] Department of Civil & Environmental Engineering, Technion – Israel Institute of Technology, Haifa 32000, Israel
[b] The Nancy and Stephen Grand Technion Energy Program and Department of Civil & Environmental Engineering, Technion – Israel Institute of Technology, Haifa 32000, Israel

ARTICLE INFO

Keywords:
Thermoacoustic refrigerator
Thermoacoustic heat pump
Phase change
Wet thermoacoustics

ABSTRACT

Thermoacoustic technology is a promising approach for environmentally-friendly, low-cost heat pumping. Here, we present experiments demonstrating an acoustic-driven phase-change heat pump, and a theoretical performance analysis. An experimental setup was constructed and tested, employing a binary mixture of an 'inert' and a 'reactive' component as the working fluid. In such a system, the reactive component undergoes evaporation and condensation as part of the acoustic cycle, resulting in latent heat transfer that augments the overall heat flux. In order to further characterize the performance of such a system, a mathematical model of the thermoacoustic heat pump was employed. Experiments generally demonstrate that a larger cooling power and a higher *COP* can be obtained with phase change, compared with a classical system. However, this enhancement is only maintained as long as the temperature difference does not exceed a 'critical' value. Otherwise, the time-averaged mass flux reverses its direction and thereafter carries heat against the heat pumping direction. This critical temperature difference is proportional to the value of the local acoustic impedance. We found that increasing the acoustic impedance by locally enlarging the cross-sectional area of the stack, resulted in better performance and enabled an increased temperature difference. Further, a high concentration of the reactive component is required for efficient operation. For instance, a COP above 40% of the Carnot COP can theoretically be obtained when the heat pump is operated with isopropanol at a concentration of ~0.8, at a temperature difference of 30 °C.

1. Introduction

According to a recent estimate made by the International Institute of Refrigeration, the number of devices for household and industry refrigeration and heat pumping in the world is around three billion, amounting to 18% of the total electricity consumption [1]. Most of these devices are based on vapor-compression technology, that still largely relies upon conventional refrigerants that negatively impact the environment via their contribution to climate-change and ozone depletion. These conventional refrigerants are in a phase-down scenario; meanwhile, other cost-effective, environmentally-benign technologies for heat pumping are required [2]. A thermoacoustic heat pump is based on the transport of heat generated by acoustic power, due to the interaction between pressure, density and temperature in the acoustic field. It has been listed by the U.S. Department of Energy as one of the possible replacements to vapor-compression cooling, due to its high efficiency, low cost and environmentally-benign operation [3].

A typical thermoacoustic heat pump consists of four sections: (1) a porous material that increases the solid–gas contact area, referred to as a 'stack' or regenerator; (2) a resonator in which the acoustic field is maintained; (3) heat exchangers for extracting the cooling power or rejecting heat; and (4) a sound source. In principle, the only section that may involve moving parts is the sound source. However, if the sound is generated by a thermoacoustic engine or piezoelectric actuator, the device will have no moving parts. This exceptional characteristic makes the thermoacoustic heat pump highly reliable and virtually maintenance-free, exemplified by its use in space applications [4]. Other applications including natural gas liquefaction [5,6], electronic device cooling [7], and food household use [8,9] have also been reported.

The performance of a heat pump is normally described using the coefficient of performance (COP), which in this case is defined as the ratio of cooling power to the consumed energy. A typical experimental value of the COP_R (defined as the ratio of *COP* over the corresponding, Carnot COP), for an optimised thermoacoustic heat pump is between

* Corresponding author.
E-mail address: ramong@technion.ac.il (G.Z. Ramon).

https://doi.org/10.1016/j.enconman.2021.113848
Received 6 November 2020; Accepted 9 January 2021

10% and 16% for a standing-wave system [10,4] and can reach ~20% for a travelling-wave system [11]. Some heat-driven thermoacoustic heat pumps can reach an overall COP_R of above 10% of the Carnot cycle when the cooling stage works in the cryogenic temperature range [12,5]. For comparison, the typical COP_R of a commercially available, household air conditioner is ~20%–30% [13], and the highest COP_R achieved in the lab is 60% [14]. For some other alternatives to vapor compression technology (e.g., thermoelectric, thermionic, magnetic, etc.), the values of COP_R achieved are generally below 20% [14].

However, after more than four decades of research, very little improvement on classical thermoacoustic heat pumps can be expected [15]. A promising approach, with the potential to break through the current limitations, is to incorporate mass transfer (e.g., phase change, adsorption, absorption, etc.) into thermoacoustic conversion [16–20]. By adding a 'reactive' component, which enables the gas mixture to exchange mass with the sorbent layer coated on the solid surface (or simply evaporate(condense) from(onto) the solid surface) during the thermoacoustic cycle, a time-averaged mass flux of the reactive component will emerge, in turn carrying significant amounts of latent heat [21,17]. This heat flux may either enhance the heat pumping or diminish it, depending on the direction of the mass flux. Slaton et al. [16] revealed that the direction of the mass flux depends on the temperature gradient, illustrated via an idealized model of a standing-wave heat pump with phase change. The direction of the mass flux will be up the temperature drop if the temperature gradient is smaller than a critical value (see Eq. (9)), therefore increasing the amount of heat pumped, or vice versa. Hence, the addition of mass exchange may improve the performance of the heat pump if temperature gradient is in the correct range.

To date, both experimental verification and full theoretical modelling of a thermoacoustic heat pump incorporating phase change have yet to be carried out. Herein, we experimentally characterize a phase-change thermoacoustic heat pump (PTHP) that incorporates a binary mixture comprising an 'inert' gas and a 'reactive' species which undergoes condensation and evaporation during the thermoacoustic cycle. Systematic experiments were performed to investigate the performance of the PTHP with different reactive components, and a comparison was made with the case of an inert gas only, i.e., with no phase change. Full numerical calculations, based on linear theory, were then used to explore the heat pump performance under various mean pressures and concentrations. Our results illustrate the potential of phase change systems for significantly increased COP_R and cooling power of the thermoacoustic heat pump.

2. Experimental setup

The experimental system designed to test the PTHP consists of a loudspeaker, a resonator and a thermoacoustic core (including a cold heat exchanger, a stack and an ambient heat exchanger), placed inside the resonator near the velocity node, i.e., the right end (see schematic in Fig. 1 and a picture of the system can be found in Fig. S1 in the supplementary material). The length and diameter of the resonator are 0.88 m and 47 mm, respectively, and the stack is a piece of 600-CPSI (cells per square inch) ceramic honeycomb with a length of 95 mm. The ambient heat exchanger is a plate-fin type, with a spacing of 2 mm and fin width of 0.7 mm. The cold heat exchanger is a screen mesh made of 0.5 mm-thick nickle-chrome wire, embedded within a 3D-printed skeleton, to provide the heat load into the system. The system is driven by a loudspeaker at the resonant frequency of the system, found to be 86 Hz. For a complete list of specifications and system dimension, please refer to Table 1.

Atmospheric air was used as the inert gas, while water or isopropanol was tested as the reactive component. In the 'wet' mode experiments (with phase change), the stack was immersed in the reactive component for 15 minutes before the experiments, to provide a source of the reactive component on the surface of the stack. The stack channels were then cleared of liquid, which only remained absorbed within the porous channel walls. In contrast, for the 'dry' mode experiments (classical thermoacoustic experiments), the stack was first dried (at 140 °C for 30 minutes), to ensure no reactive component remained on it. This procedure is important, because even a little bit of humidity, either from the reactive component remained on the stack or the ambient air, can create significant noise in the dry mode experiments. The stack section was thermally insulated by polystyrene foam. In order to reduce the influence of heat loss to the ambience, the ambient temperature was kept at 25 °C in all experiments by adjusting an external recirculating chiller connected to the ambient heat exchanger.

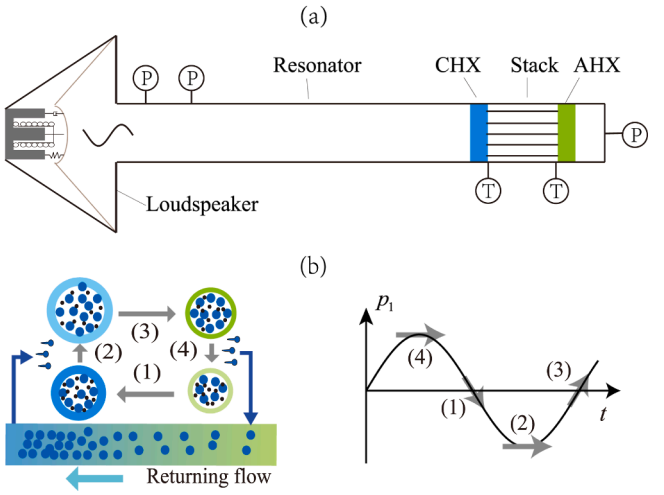

Fig. 1. (a) Schematic of the phase-change thermoacoustic heat pump. The system consists of a loudspeaker, a stack sandwiched by a cold heat exchanger and an ambient heat exchanger, and a resonator. The symbols 'CHX' and 'AHX' stand for the cold heat exchanger and the ambient heat exchanger respectively. 'P' and 'T' represent pressure sensors and thermocouples respectively. (b) The left figure presents thermodynamic cycle of the phase-change standing-wave thermoacoustic conversion; the right figure shows the corresponding pressure amplitudes. The black and blue dots represent the inert and reactive molecules, respectively. The four thermodynamic steps are: (1) adiabatic expansion, (2) isobaric heat absorption with mass gain, (3) adiabatic compression and (4) isobaric heat rejection with mass loss.

Table 1
Specifications of the phase-change thermoacoustic heat pump.

Items	Dia. (mm)	Lg. (mm)	Details
Cold heat exchanger	47	5	A heating filament made of 0.5-mm thickness nickle-chrome wire (8.6 ohm), embedded in a 3D printed skeleton
Stack	47	95	600 CPSI ceramic honeycomb
Ambient heat exchanger	47	10	Parallel-plates heat exchanger, gap width is 2 mm, fin width is 0.7 mm
Resonator	47	880	–
Loudspeaker	–	–	Cerwin-Vega V84DV2. Its frequency and volume are controlled through a waveform generator and an amplifier

When in operation, the mixture parcels in the PTHP undergo a thermodynamic cycle of the standing-wave thermoacoustic heat pump with phase change, whose conceptual representation is shown in Fig. 1b. The cycle begins from Step (1), in which the fluid 'parcel', a mixture of the reactive component and the inert gas, moves toward the low pressure region while expanding adiabatically. In Step (2), the lowered partial pressure drives evaporation of the reactive component from the solid surface into the parcel, carrying latent heat with it. In Steps (3) and (4), the parcel undergoes the reverse processes of steps (1) and (2), whereby the parcel moves back along the direction of wave propagation

and the reactive component condenses on the solid, transferring the latent heat. Mass, and latent heat, are therefore shuttled along the stack, creating and maintaining a temperature difference. In this 4-step cycle, the acoustic power is consumed in order to pump heat against the temperature gradient. As shown in the figure, there is a time-averaged mass flux from cold end to hot end, which contributes to the heat flux. However, under large temperature difference, the direction of the mass flux reverses and hinders the heat pumping. The direction of mass flux is a key point for the performance of a phase-change thermoacoustic heat pumping, which will be further discussed in Section 4.2.

The acoustic power supplied by the loudspeaker, $\dot{E}_l$, was measured by two pressure sensors (Endevco 8510B-2), installed at a distance of 18 cm from each other (for details of this method, see [22]). Another pressure sensor was installed at the right end of the resonator, which corresponds with the point of maximal pressure amplitude (anti-node). Two K-type thermocouples, installed at the two ends of the stack, were used to measure the cold temperature, T_c, and ambient temperature, T_a. The cooling power was measured by a Rigol DP832 power supply. The errors of measured temperature, pressure amplitude, acoustic power and cooling power have be analysed in the supplementary material.

3. Theoretical model

The theory describing thermoacoustic conversion with phase change was first developed by Raspet et al. [23] and Slaton et al. [16] who introduced the effects of phase change and mass diffusion into linear thermoacoustic theory. Recently, this theory was expanded by Weltsch et al. [17] and Offner et al. [21] to include reversible reactions such as absorption or adsorption. Here, we use the dimensional forms of the governing momentum, continuity and energy balance equations as given in Offner et al. [21]:

$$\frac{dp_1}{dx} = -\frac{i\omega\rho_m}{F_\nu A_{\mathrm{gas}}}U_1, \tag{1}$$

$$\frac{dU_1}{dx} = -\frac{i\omega A_{\mathrm{gas}}}{\rho_m a^2}\left[\gamma + F_\alpha\left(1-\gamma\right) + \gamma\frac{C_{\mathrm{m}}}{1-C_{\mathrm{m}}}\frac{1-F_D}{\eta_{\mathrm{D}}}\right]p_1 + \left[\frac{F_\nu - F_\alpha}{(1-Pr)F_\nu}\beta + \frac{\frac{\eta_\nu}{\eta_{\mathrm{D}}}(1-F_D)-(1-F_\nu)}{F_\nu(1-Sc)}\frac{C_{\mathrm{m}}}{1-C_{\mathrm{m}}}\frac{l_{\mathrm{h}}}{R_{\mathrm{g}}T_{\mathrm{m}}^2}\right]\frac{dT_m}{dx}U_1, \tag{2}$$

$$\frac{dT_m}{dx} = \frac{\dot{H}_2 - \frac{1}{2}\Re\left[p_1\widetilde{U}_1\left(1-\frac{\widetilde{F}_\nu - F_\alpha}{(1+Pr)F_\nu}\right)\right] - \dot{m}l_{\mathrm{h}}}{\frac{\rho_m c_p|U_1|^2}{2A_{\mathrm{gas}}\omega(1-Pr)|F_\nu|^2}\Im\left[\frac{\widetilde{F}_\nu - F_\alpha}{1+Pr} - \widetilde{F}_\nu\right] - \left(A_{\mathrm{gas}}k + A_s k_s\right)}, \tag{3}$$

in which p_1 and U_1 are the amplitudes of the pressure and volumetric velocity, respectively, while T_m and ρ_m denote the mean temperature and density of the mixture, respectively. In addition, a is the speed of sound, c_p is the heat capacity, γ is the heat capacity ratio, β is the thermal expansion coefficient, R_g is the universal gas constant, ω is the angular frequency. k and k_s denote the thermal conductivity of the gas and solid, respectively, and l_h is the latent heat of the reactive component, A_{gas} and A_s represent the cross-sectional area for gas and solid, respectively, while Pr is the Prandtl number and Sc is the Schmidt number. The symbols $\Re$ and $\Im$ denote the real and imaginary parts of a complex number, respectively. Finally, $\dot{m}$ is the time-averaged mass flux generated by phase change in the oscillatory flow, given by [17]

$$\dot{m} = \frac{1}{1-C_{\mathrm{m}}}\frac{C_{\mathrm{m}}}{2R_{\mathrm{g}}T_{\mathrm{m}}}\Re\left[p_1\widetilde{U}_1\frac{F_{\mathrm{D}}-\widetilde{F}_\nu}{\left(1+Sc\right)\widetilde{F}_\nu}\right] - \frac{1}{1-C_{\mathrm{m}}}\frac{|U_1|^2}{2A_{\mathrm{gas}}\omega|F_\nu|^2}\frac{p_{\mathrm{m}}C_{\mathrm{m}}l_{\mathrm{h}}}{R_g^2T_{\mathrm{m}}^3}\frac{1}{1-Sc^2}\Im\left[\widetilde{F}_\nu\left(1+Sc\right) + \frac{\eta_\nu}{\eta_{\mathrm{D}}}\left(F_{\mathrm{D}}-\widetilde{F}_\nu\right)\right]\frac{dT_{\mathrm{m}}}{dx} - \frac{p_{\mathrm{m}}A_{\mathrm{gas}}D}{1-C_{\mathrm{m}}}\frac{C_{\mathrm{m}}l_{\mathrm{h}}}{R_{\mathrm{g}}^2T_{\mathrm{m}}^3}\frac{dT_{\mathrm{m}}}{dx}, \tag{4}$$

where D is the diffusion coefficient. The functions F_n ($n = \alpha, \nu$ or D) for a honeycomb stack with rectangle channel are defined as [24]:

$$F_n = \frac{64}{\pi^4}\sum_{\substack{m_1 m_2 \\ \mathrm{odd}}}\frac{1}{m_1^2 m_2^2\left(1-\frac{i\pi^2}{16(p+q)^2\tau_n^2}\left(q^2m_1^2+p^2m_2^2\right)\right)}, \tag{5}$$

where p and q are the length and the width of the channel. m_1 and m_2 are odd numbers, $\alpha \equiv k/\rho c_p$ is the thermal diffusivity, ν is the kinematic viscosity, and $\tau_n = r_h\sqrt{\omega/n}$, in which r_h represents the hydraulic radius, is a dimensionless number representing the ratio of diffusive time scales (for conduction, momentum and mass diffusion, respectively) and the oscillation time scale.

The mixture in the stack is assumed to be at equilibrium with the liquid on the solid wall. Therefore, the mean concentration C_m can be calculated using the Clausius–Clapeyron relation:

$$C_m = \exp\left[-\frac{\mathrm{l_h}}{\mathrm{R_g}}\left(\frac{1}{\mathrm{T_m}}-\frac{1}{\mathrm{T_b}}\right)\right] \tag{6}$$

where T_b is the boiling temperature of the reactive component.

Eqs. (1)–(3) define a boundary value problem of three coupled, nonlinear ordinary differential equations. At the closed end on the right side of the system, a no-penetration boundary condition, i.e., $U_1 = 0$, is imposed. The second boundary condition is imposed by setting the pressure amplitude at the closed end. In the calculations aimed at comparing model calculations with experimental measurements, the pressure amplitude is set according to the experimentally measured value. In all other calculations, it is set at 8% of the mean pressure. The equations are solved using a fourth-order Runge–Kutta routine beginning at the loudspeaker, along with a shooting method that targets the boundary conditions at the closed end. The numerical solution provides the distributions of p_1, U_1, T_m and $\dot{H}_2$ along the system. The acoustic power is calculated by $\dot{E}_2 = \frac{1}{2}\Re[\widetilde{p_1}U_1]$. The pumped heat is determined through the energy balance at the ambient heat exchanger, i.e., $Q_c = \dot{H}_2 - \dot{E}_2$ [22]. Note that the loudspeaker in calculation was arbitrarily considered ultracompliant, which provides a boundary representing a pressure node and velocity antinode [25,4]. Therefore, the frequency was adjusted so that the oscillation in the resonator was always in a quarter wavelength resonance. The heat transfer coefficient between the solid wall of the heat exchanger and the fluid is assumed to be infinite, representing an ideal heat exchanger.

In order to evaluate the performance of the heat pump, we define the coefficient of performance of the system

$$COP = \frac{Q_{\mathrm{c}}}{\dot{E}_l} \tag{7}$$

where $\dot{E}_l$ is the acoustic power consumed by the PTHP, which is equal to the acoustic power supplied by the loudspeaker. We also define a coefficient of performance relative to the corresponding Carnot cycle

$$COP_R = COP\frac{T_a - T_c}{T_c} \tag{8}$$

where T_a and T_c are the temperatures at the ambient and cold ends of the stack.

4. Results and discussion

4.1. Experimental performance of the heat pump

We begin with the experimental comparison between the two modes of the heat pump, that is, with phase change ('wet') or without it ('dry').

In Fig. 2a, we present the experimental measurements of the cooling power, Q_c, achieved at varying temperature difference, ΔT, and constant pressure amplitude at the closed end on the right side of the system. We find that the wet mode (using isopropanol or water) sustains higher cooling loads compared with the dry mode, when $\Delta T < 10°C$. This is because the phase change of isopropanol/water enhances the thermoacoustic conversion through latent heat transfer. Further, the Q_c achieved with isopropanol is generally higher than water, due to the higher concentration of isopropanol at the ambient side, $C_{m,a}$, which is twice that of water. A higher concentration means that more mass is exchanged during each oscillation cycle, leading to a larger heat flux. Results also show that as ΔT increases, the Q_c achieved decreases faster in the wet mode than in the dry mode. As a result, both the dry mode and the wet mode (with both isopropanol and water) are unable to pump heat beyond $\Delta T \sim 11°C$. The reason for this is that, inherently, the mass flux assisting heat pumping due to phase change decreases as ΔT increases, until it eventually reverses its direction to work against the heat pumping, leading to a similar or even lower performance compared with the dry mode. Further, since the values of input acoustic power supplied by the loudspeaker are ~ 1.5 W in all experiments, the trends of COP are similar to those shown for Q_c. The highest COP_R in the experiments is 3.3% when isopropanol is used with $\Delta T = 6°C$, which is three times higher than the equivalent dry case. Our results clearly show that phase change helps improve the performance as long as ΔT is smaller than a critical value, which is around 10—11°C in the experiments. Note that, typically, a dry mode standing-wave thermoacoustic refrigerator in the literature could reach a COP_R above 10% when the mean pressure is $\sim$ 10 bar [4], while the experimental values of COP_R in this work are much lower. The main reasons are that the current system is limited to work at the atmospheric mean pressure, and the cross-sectional area of the stack is far from the optimal value. The optimisation of these will be discussed further in Section 4.2. Additionally, we compared the cooling power when the system was positioned horizontally and vertically, the results show that the orientation of the system has little effect on its performance (see Fig. S3 in the supplementary material).

Alongside the experimental results, we also show the corresponding model calculations, carried out based on the experimental conditions, in Fig. 2b. While showing reasonable quantitative agreement, the calculated values of Q_c are higher than those in the experiments for the same ΔT, and this deviation increases as ΔT is increased. For example, when $\Delta T \sim 0$ °C, the calculated values of Q_c are 1 W, 1 W and 0.9 W higher than the corresponding experimental values for water, isopropanol and dry cases, respectively. However, when $\Delta T \sim 10$–11 °C, the calculated values of Q_c are 2–3 W, while the experimental results drop to ~ 0 W. The deviations are mainly attributed to heat losses through the wall of resonator, unaccounted for in the model. In the experiments, there are temperature gradients along the resonator in both the stack section and the section to the left of the cold heat exchanger, through which part of the cooling power is 'wasted' – the lower the cold side temperature, the stronger this effect.

4.2. Model-based performance projection

The present experimental system is mainly used as a proof-of-concept, and would require significant optimisation in order to achieve good performance that can be bench-marked against existing heat pump technology. In particular, as mentioned previously, it is limited to atmospheric mean pressure and low concentrations of the reactive component. In order to look beyond the experimental limitations, we use the theoretical model to probe further into the performance characteristics of the PTHP.

4.2.1. Heat-pump performance with and without phase change

We begin by comparing the performance of the PTHP in both dry and wet modes. In standing-wave thermoacoustic systems, a value of $\tau_\nu > 1$ is required, so that the oscillation time scale is comparable to that for diffusion between the fluid parcel and the solid wall, which enables the proper phase-lag that facilitates the time-averaged mass streaming [16,17]. Accordingly, we observe that the value of COP_R rises as τ_ν is increased, and it reaches a plateau at $\tau_\nu \sim 2.5$ for both wet and dry modes (not shown in the figure). The COP_R of both modes is shown in Fig. 3a, and the ratio of cooling power in the wet mode over that in the

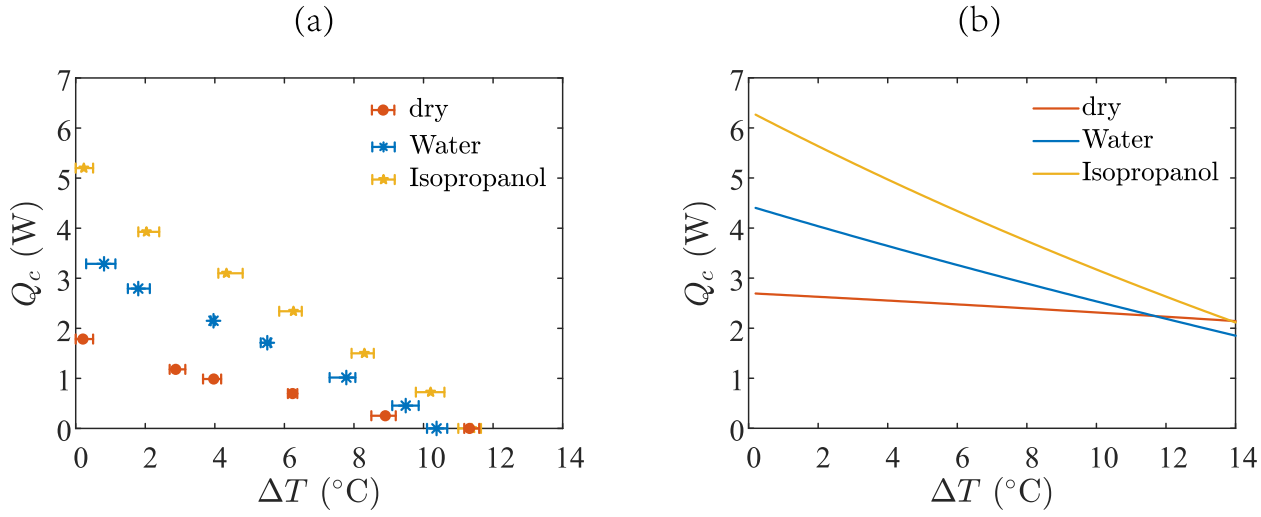

Fig. 2. The dependence of cooling power on temperature difference. (a) Experimental results. (b) Calculated results. The results for the dry case is compared with the wet case with either isopropanol or water as the reactive component. The ambient temperature was fixed at 25°C. In all experiments, the input acoustic power were kept at ~ 1.5 W..

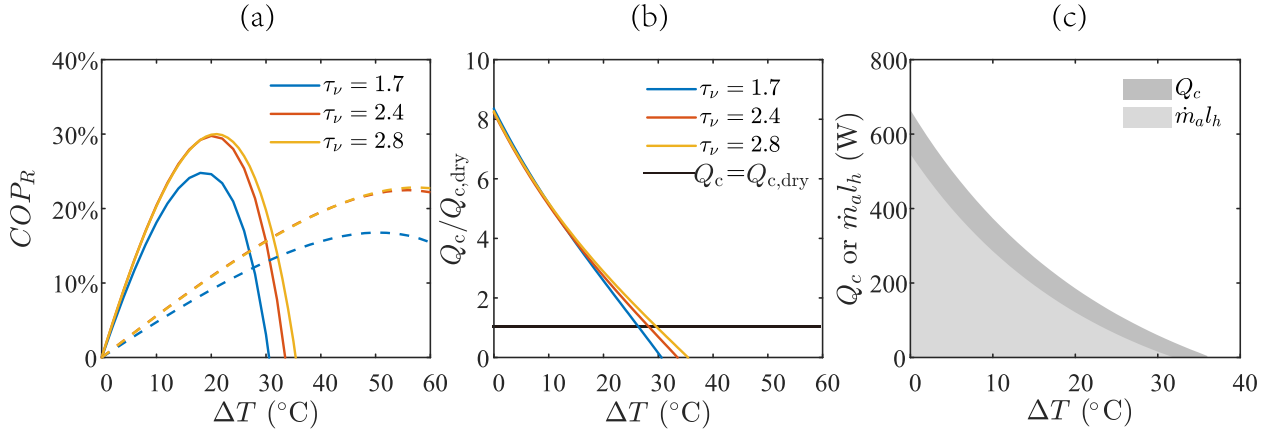

Fig. 3. Heat pump performance, comparing wet (with phase change) and dry modes. (a) The dependence of COP_R on ΔT with different τ_ν ($\tau_\nu = r_h\sqrt{\omega/\nu}$). The solid and dashed lines represent wet and dry modes respectively. (b) The ratio of cooling powers in the two modes vs. ΔT, with different τ_ν. (c) The contribution of the latent heat carried with the mass flux $\dot{m}_a l_h$, and cooling power Q_c, vs. ΔT $C_{m,a} = 0.4$ The inert gas is air and, in the wet mode, the reactive component is isopropanol. The value of $|p_1|$ at the velocity node is set to be 8% of the mean pressure.

dry mode is shown in Fig. 3b, under three representative values of τ_ν. As was observed experimentally, both the COP_R and Q_c are much higher in the wet mode than the equivalent cases in the dry mode, until ΔT passes some critical value. Recall that the difference between the two modes is essentially the heat flux generated by the time-averaged mass flux $\dot{m}$, generated through the phase change. However, the presence of this extra heat flux improves performance only when it is directed against the temperature drop. For a standing-wave system, the first and second terms in Eq. (4), representing thermoacoustic 'pumping' and hydrodynamic dispersion, respectively, have opposing signs and the competition between them determines the overall direction of $\dot{m}$; the third term, representing diffusion, is generally much smaller than the others and may be ignored. When ΔT is small, the first term is dominant, leading to a mass flux against the temperature drop, augmenting the heat pumping. As ΔT is increased to a critical value, the magnitude of the dispersion term surpasses the pumping term, resulting in reversal of the mass flux, carrying heat from the hot end to the cold end. This inevitably reduces the efficiency of the heat pump and so the COP_R in the wet mode becomes lower than in the dry mode. The contribution of the latent heat, carried with the mass flux, to the overall heat flux, is also shown in Fig. 3c. Note that $\dot{m}_a$ is the spatially-averaged mass flux, along the stack, generating a heat flux $\dot{m}_a l_h$. The results show that the pumped heat contributed by the mass flux, $\dot{m}_a l_h$, accounts for a large portion of the total cooling power Q_c, and this contribution decreases as ΔT is increased. For instance, the ratio of $\dot{m}_a l_h$ over Q_c is 82% when $\Delta T \sim 0$ °C, while it drops to 65% when $\Delta T = 20$ °C, for $\tau_\nu = 2.8$. Eventually, $\dot{m}_a l_h$ becomes negative when $\Delta T > 32$ °C, at which point the presence of phase change becomes detrimental to the heat pumping process. In fact, the values of ΔT at which wet and dry modes have identical COP_R and Q_c are very close to the ΔT at which $\dot{m} l_h = 0$. We also note that the acoustic fields for both dry and wet modes are very similar, as manifested in the distributions of phase difference ϕ and acoustic impedance Z along the resonator (see Fig. S4 in the supplementary material). This excludes the possibility that the increased performance in the wet mode is caused by some improvement of the acoustic field. Moreover, the corresponding input acoustic power may be as high as 80 W, which exceeds the output ability of a typical loudspeaker. Therefore, a more powerful sound source like a linear alternator should be used.

4.2.2. *Increased acoustic impedance in the stack increases the temperature range*

As discussed previously and shown in Fig. 3, the performance of the PTHP is severely limited by the critical temperature difference ΔT_{crit}, at which the mass flux is zero. By setting $\dot{m} = 0$ in Eq. (4), assuming an ideal standing wave field and no diffusive losses, an approximate expression of the critical temperature gradient in a short stack (i.e., variation of p_1, U_1 and T_m can be ignored along the axial direction) can be achieved

$$\nabla T_{crit,id} = \frac{\gamma}{\gamma - 1}\frac{R_g T_m \omega |Z|}{l_h c_p \rho_m}. \tag{9}$$

This expression was first derived by Raspet et al. [16]. It indicates that the critical temperature difference can be extended by increasing the acoustic impedance $|Z| = |p_1 A_{gas}/U_1|$, which may be achieved by locally enlarging the cross sectional area of the stack (see Fig. 4a). To test this concept, we compare the heat pump performance with four different cross-sectional areas of the thermoacoustic core ranging from A_r to $5A_r$, where A_r is the cross-sectional area of the resonator. As shown in Fig. S5 in the supplementary material, the mean value of the acoustic impedance, averaged along the stack, $|Z|_a$, can be increased effectively by enlarging the cross-sectional area of the thermoacoustic core. For instance, when $\Delta T = 30$ °C, the values of $|Z|_a/\rho_m a$ along the stack are 5.2, 7.4, 8.7 and 10.6 for the cross-sectional area of A_r, $2A_r$, $3A_r$ and $5A_r$, respectively. Consequently, ΔT_{crit} rises from 35 °C to 60 °C (see Fig. 4c) when the cross-sectional area A_c is increased from A_r to $5A_r$. The value of $\dot{m}_a l_h$ at a large ΔT is also significantly increased, leading to a higher COP_R (see Fig. 4b). For example, $\dot{m}_a l_h < 0$ when $\Delta T = 35$ °C with the cross-sectional area of $A_c = A_r$, while it is increased to 66 W with the cross-section area of $A_c = 2A_r$, leading to a COP_R increase from around 0 to 31%. We also note that the influence of A_c also depends on the mean pressure, previously discussed in the context of increased performance through a higher power density. As shown in Fig. 4d, a smaller p_m requires a larger A_c to maintain equal performance. The values ofA_c/A_r yielding the highest COP_R for mean pressures of 1 bar, 5 bar and 10 bar are 2, 2.9 and 3.8, respectively.

4.2.3. *The importance of the reactive component mean concentration*

A vital parameter for the performance of the phase-change heat pump is the mean concentration of the reactive component, C_m. From Eq. (4), we see that $\dot{m} \propto C_m/(1 - C_m)$, hence a higher C_m means that phase change plays a more important role in the thermoacoustic conversion. C_m also significantly influences the variation of U_1 according to Eq. (2), and further affects the variation of p_1 and T_m. Furthermore, the properties of the mixture also depend on C_m.

In the calculations shown previously, the concentration at the

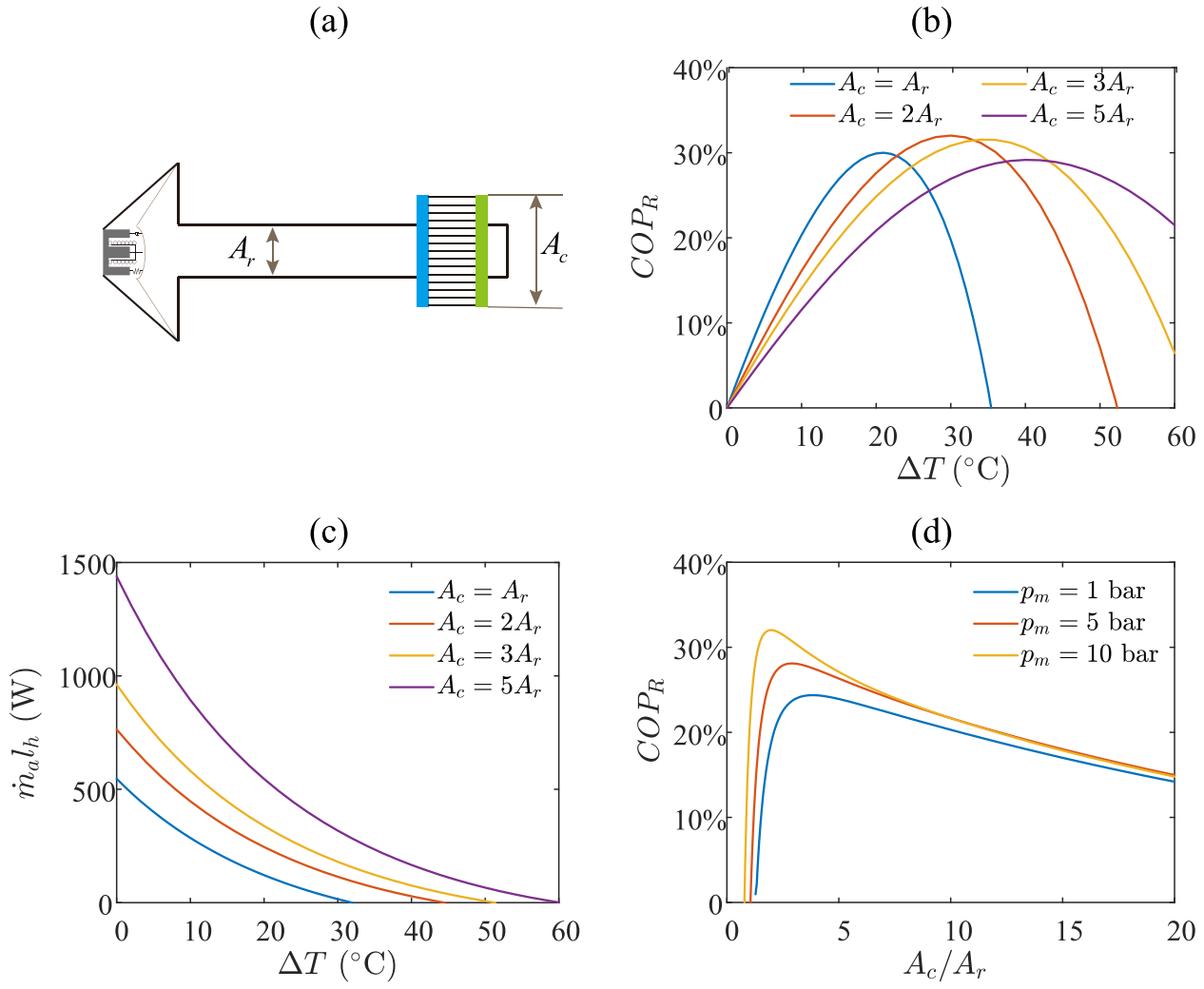

Fig. 4. Influence of the cross sectional area of the thermoacoustic core on the performance of the PTHP. (a) Schematic of the system with an enlarged thermoacoustic core. (b) The dependence of COP_R on ΔT with different values of A_c. (c) The dependence of $\dot{m}l_h$ on ΔT with different values of A_c. (d) The dependence of COP_R on A_c/A_r with different mean pressure. The reactive component is isopropanol. $C_{m,a} = 0.4$. $\tau_\nu = r_h\sqrt{\omega/\nu} = 2.8$. The value of $|p_1|$ at the velocity node is set to be 8% of the mean pressure.

ambient end $C_{m,a}$ was fixed at 0.4. In Fig. 5, we present the performance of the system with $C_{m,a}$ varied from 0.1 to 0.95, and with different reactive components, while ΔT is fixed at 30 °C. As may be seen, COP_R steadily increases with $C_{m,a}$, reaching a peak value at high $C_{m,a}$ (0.8–0.9), before decreasing somewhat. The highest COP_R, > 40%, can be achieved when isopropanol is used. Note that 20%– 30% of the total acoustic power is dissipated in the resonator. If we ignore this loss, which may be minimized through possible acoustic optimization, the COP_R can reach above 50% when $C_{m,a} \sim 0.8$ for isopropanol. The COP_R for a system containing isopropanol is higher than that with water at the same $C_{m,a}$ and p_m, because isopropanol has lower values of Pr, Sc and ν, and hence reduced viscous losses. A higher value of Q_c can be achieved with water at the same mean pressure and $C_{m,a}$, because of the larger latent heat. The results in Fig. 5 further demonstrate an advantage of a phase-change thermoacoustic system over the classical system, in which a high mean pressure is necessary to achieve high efficiency and power density.

4.2.4. Suggested reactive components for different working temperatures and mean pressures

Yang et al. [26] suggested five factors for evaluating the working fluid of a phase-change thermoacoustic system: the boiling temperature T_b and the parameter ψ of the reactive component; the Prandtl number Pr, the Schmidt number Sc and the kinematic viscosity ν of the mixture of inert and the reactive components. ψ is defined as

$$\psi = \frac{C_m}{1 - C_m}\frac{l_h}{R_g T_m}. \tag{10}$$

Note that the acoustic sink term, which represents the acoustic-to-thermal conversion, can be written as $g = g_{dry}(1 + \psi)$, where g_{dry} is the acoustic sink term in the classical thermoacoustic heat pumping (see supplementary material). Therefore, ψ represents the potential power of phase change in the thermoacoustic conversion. Among the five factors mentioned above, T_b and ψ of the reactive component are more important because the former determines the temperature range the thermoacoustic system working within, and the latter indicates whether the effect of phase change is significant. Further, as discussed previously in Fig. 5, the PTHP can work efficiently with a high concentration of the reactive component. This, in turn, 'confines' the system to appropriate working temperature and mean pressure ranges for a specific reactive component. Therefore, it is necessary to investigate reactive components applicable for different working temperatures and mean pressures.

As an illustration of the possible choices for different temperature and mean pressure ranges, we consider 9 substances as the reactive component (see Fig. 6, note that these substances are used as the reactive component respectively). The areas marked for each reactive

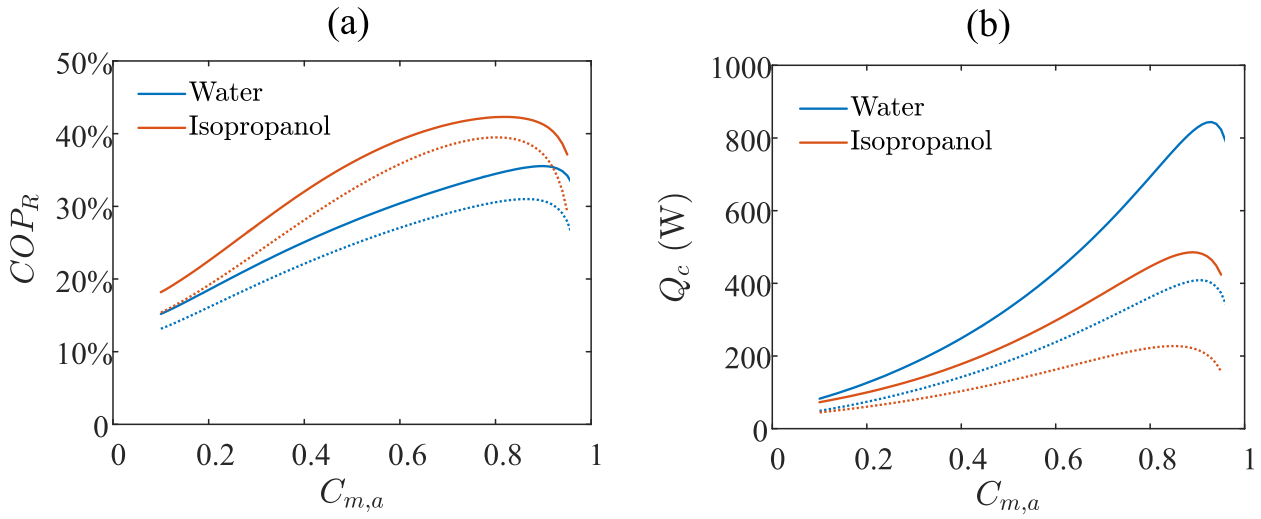

Fig. 5. The dependence of the performance on the concentration of reactive component at the ambient side, with isopropanol and water as the reactive components. (a) COP_R vs. $C_{m,a}$. (b) Q_c vs. $C_{m,a}$. The solid and dashed lines represent the results under mean pressures of 10 bar and 5 bar respectively. $\Delta T = 30\,^{\circ}\mathrm{C}$, $\tau_\nu = r_h\sqrt{\omega/\nu} = 2.8$. The solid and dotted lines represent results for $p_m = 10$ bar and $p_m = 5$ bar, respectively. $A_c = 2A_r$ for $p_m = 10$ bar, $A_c = 2.9A_r$ for $p_m = 5$ bar, according to the results in Fig. 4. The value of $|p_1|$ at the velocity node is set to be 8% of the mean pressure.

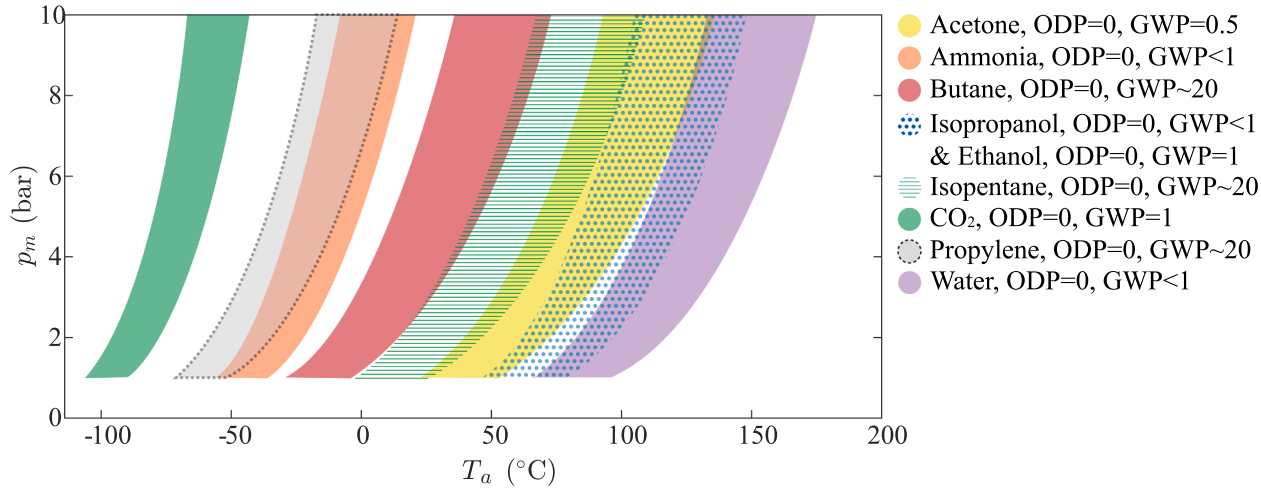

Fig. 6. Suggested reactive components and their efficient working ranges of pressure and temperature. The areas for different reactive components are confined by $\psi > 5$. A limit of $C_m < 0.9$ is arbitrarily set, to avoid the risk of temperature arising to the boiling temperature due to pressure oscillations or fluctuations in heat load, which significantly accelerates the evaporation. Note that the areas for isopropanol and ethanol are combined because they have similar properties. ODP and GWP of acetone, ethanol and isopropanol are from Ordaz-Flores et al. [30], Pantaleo et al. [31] and Burkholder et al. [32] respectively. Other data are from Calm and Hourahan [33].

component cover the temperature and mean pressure ranges for which $\psi > 5$, to ensure a significant effect of phase change in the thermoacoustic conversion. The temperature T_m exhibits a complicated effect on ψ (see Eq. (10)). On the one hand, $\psi \propto T_m^{-1}$, thus a large value of ψ can be achieved for a reactive component with low boiling temperature even without a high l_h. For example, l_h of ammonia at atmospheric pressure is only 57% of that for water, but the values of ψ of these two substances are similar at a given C_m. On the other hand, according to Eq. (6), when the boiling temperature is lower, the value of C_m, which is also a determining factor of ψ, becomes more sensitive to the variation of T_m. Consequently, the operational range for the more volatile reactive components (e.g., CO_2, propylene and ammonia), is narrower than for other reactive components. Additionally, in the classical thermoacoustic systems, the increase of mean pressure is often helpful to improve the performance [27]; however, here we see that there exists an upper limit of mean pressure for efficient operation in phase-change thermoacoustic systems. This is because the increase of the mean pressure will reduce C_m, as well as ψ, and thus may lower the performance of the PTHP.

The suggested working areas for different reactive components with different boiling temperatures in Fig. 6 cover a wide temperature range—from applications of industrial high-temperature heat pumps to near-cryogenic coolers. Therefore, the appropriate reactive component can be selected according to the temperature range and mean pressure of the system. If there are multiple choices, values of Pr, Sc and ν should also be taken into consideration – smaller values are preferred for reducing viscous losses. We note that a reactive component with lower boiling temperature might help reduce the viscosity of the mixture, because the viscosity of the inert component decreases as temperature decreases. For example, at $p_m = 1$ bar and $C_m = 0.4$ with air as the inert component, the value of ν with ammonia as the reactive component is only 42% of that with water. Environmental issues such as ODP (ozone depletion potential) and GWP (global warming potential) of the reactive

component should then be taken into consideration. All of the selected species shown here (this is a non-exhaustive list and there may be other, potentially better materials) are safe for the ozone layer (zero ODP), and exhibit very low values of GWP.

Additionally, the inert component is also a determining factor of the properties of the mixture, as well as the frequency of the system. Generally, environmentally friendly gases, including but not limiting to air, nitrogen, helium and argon, can be used. The selection of the inert component is independent of the reactive component, and the criterion has been extensively discussed in Belcher et al. [28] and Tijani et al. [29].

5. Concluding remarks

Herein, we presented a novel, efficient heat pump based on phase-change heat transfer in an acoustic field, with the working fluid of a binary mixture including an inert gas (air) and a reactive component (water or isopropanol) that undergoes reciprocating condensation and evaporation used as the working mixture. We built an acoustic-driven standing-wave thermoacoustic heat pump, and the corresponding numerical model.

Our experimental results show that a larger cooling power and a higher *COP* can be obtained with phase change when the temperature difference is below a critical value, which verifies that the phase change enhances thermoacoustic heat pumping. However, when the temperature difference is increased to exceed the critical value, the performance becomes worse than the equivalent classical thermoacoustic heat pump, because the time-averaged mass flux reverts its direction and carries heat against the heat pumping direction. This critical temperature difference (or gradient) is proportional to the value of acoustic impedance. We find that the acoustic impedance can be increased by locally enlarging the cross-sectional area of the stack, and therefore better performance under a large temperature difference can be achieved. Further, a high concentration of the reactive component is required for efficient operation. Our calculations show that a COP >40% of the Carnot limit can be obtained with an air-isopropanol mixture at a concentration of ~0.8, at $\Delta T = 30\,^{\circ}\mathrm{C}$. Lastly, we suggested reactive components for the temperature and mean pressure in the ranges of −100–170 °C and 1—10 bar respectively.

Some technical challenges need to be overcome before the full potential of this novel heat pump can be realised. First, a better material for the stack must be found. The ceramic honeycomb used in the presented experiments may face the issues related to drying out during long-term operation. An 'ideal' stack should, therefore, meet the following requirements: Firstly, elimination of blockage due to accumulation of condensed liquid. Secondly, facilitating the continuous replenishment of liquid 'lost' via the acoustic-driven axial mass flux. Thirdly, wetting-resistance of the stack material, so as to avoid corrosion or deformation/collapse of the channel structure during long-term operation. An additional challenge lies with a high-performance heat exchanger. A significant advantage of a phase-change thermoacoustic heat pump over the traditional one is its high cooling power, which would require a heat exchanger capable of handling the expected heat loads. This may provide grounds for consideration of a heat exchanger relying on a more efficient heat transfer mechanism, e.g. phase-change or direct contact.

A phase-change thermoacoustic heat pump may be used for household and industrial heat pumping. Most importantly, it can do so with no environmentally hazardous materials and with little to no moving parts, offering potentially simple, reliable and cost-effective construction and low-maintenance operation. Furthermore, it can utilize acoustic sources driven either electrically or thermally, using accessible and abundant heat sources such as solar irradiation. As such, it offers a major technological development for a more sustainable future. Further investigation is still required for proper realization of this potential, including experimental investigation at higher mean pressure and concentration of the reactive component, as well as theoretical consideration of high-amplitude operation, beyond the linear theory adopted here.

CRediT authorship contribution statement

Rui Yang: Conceptualization, Methodology, Software, Data curation, Validation, Investigation, Writing - original draft. **Nathan Blanc:** Conceptualization, Software, Methodology, Validation, Investigation. **Guy Z. Ramon:** Conceptualization, Methodology, Supervision, Writing - review & editing, Project administration, Funding acquisition.

Declaration of Competing Interest

The authors declare that they have no known competing financial interests or personal relationships that could have appeared to influence the work reported in this paper.

Acknowledgements

This research was supported by Grant No. 219-11-127 from the Israel Ministry of Energy and Water. R.Y. was supported, in part, by a fellowship from the Israel Council for Higher Education. N.B. acknowledges the support from the Nancy and Stephen Grand Technion Energy Program (GTEP).

Appendix A. Supplementary data

Supplementary data associated with this article can be found, in the online version, at https://doi.org/10.1016/j.enconman.2021.113848.

References

[1] Coulomb D, Dupont JL, Pichard A. The role of refrigeration in the global economy. In: 29th Informatory note on refrigeration technologies. Technical Report; International Institute of Refrigeration: Paris, France.
[2] Kosmadakis G, Arpagaus C, Neofytou P, Bertsch S. Techno-economic analysis of high-temperature heat pumps with low-global warming potential refrigerants for upgrading waste heat up to 150 °C. Energy Conv Manage 2020;226:113488.
[3] William G, Zogg R, Young J, Johnson C. Energy savings potential and RD&D opportunities for non-vapor-compression HVAC technologies. Tech. Rep. DOE/EE-1021, 1220817, U.S. Department of Energy; 2014. doi: 10.2172/1220817.
[4] Garrett SL, Adeff JA, Hofler TJ. Thermoacoustic refrigerator for space applications. J Thermophys Heat Transfer 1993;7(4):595–9.
[5] Xu J, Zhang L, Hu J, Wu Z, Bi T, Dai W, Luo E. An efficient looped multiple-stage thermoacoustically-driven cryocooler for liquefaction and recondensation of natural gas. Energy 2016;101:427–33.
[6] Hou M, Wu Z, Hu J, Zhang L, Luo E. Experimental study on a thermoacoustic combined cooling and power technology for natural gas liquefaction. Energy Procedia 2019;158:2284–9.
[7] Xiao X, Gu X, Zhang X. Combination of thermoacoustic heat dissipation with oscillating convection: A novel cooling method. Int J Heat Mass Transfer 2020;160:120177.
[8] Wang H, Zhang L, Hu J, Yu G, Wu Z, Dai W, Luo E. Study on a novel looped heat-driven thermoacoustic refrigerator with direct-coupling configuration for room temperature cooling. Int J Refrig.
[9] de Blok K. Technology and application of thermoacoustic heat transformers. https://www.napnetwerk.nl/download/?id=12183; 2018 [accessed December 13, 2020].
[10] Hofler TJ. Thermoacoustic refrigerator design and performance. Ph.D. thesis, University of California, San Diego, CA; 1986.
[11] Bassem MM, Ueda Y, Akisawa A. Design and construction of a traveling wave thermoacoustic refrigerator. Int J Refrig 2011;34(4):1125–31.
[12] Xu J, Hu J, Sun Y, Wang H, Wu Z, Hu J, Hochgreb S, Luo E. A cascade-looped thermoacoustic driven cryocooler with different-diameter resonance tubes. Part: Experimental study and comparison. Energy 2020:118232.
[13] Jones WP. Air conditioning engineering. Butterworth Heinemann, 5th ed.; 2001.
[14] Brown DR, Stout T, Dirks JA, Fernandez N. The prospects of alternatives to vapor compression technology for space cooling and food refrigeration applications. Energy Eng 2012;109(6):7–20.
[15] Tartibu L. Developing more efficient travelling-wave thermo-acoustic refrigerators: a review. Sustain Energy Technol Assess 2019;31:102–14.
[16] Slaton WV, Raspet R, Hickey CJ, Hiller RA. Theory of inert gas-condensing vapor thermoacoustics: transport equations. J Acoust Soc Am 2002;112(4):1423–30, ISSN 0001-4966. doi: 10.1121/1.1508114.
[17] Weltsch O, Offner A, Liberzon D, Ramon GZ. Adsorption-mediated mass streaming in a standing acoustic wave. Phys Rev Lett 118(24), ISSN 0031-9007, 1079-7114. doi: 10.1103/PhysRevLett.118.244301.

[18] Blayer Y, Elkayam N, Ramon GZ. Phase-dependence of sorption-induced mass streaming in an acoustic field. Appl Phys Lett 2019;115(3):033703.
[19] Tsuda K, Ueda Y. Critical temperature of traveling-and standing-wave thermoacoustic engines using a wet regenerator. Appl Energy 2017;196:62–7.
[20] Senga M, Hasegawa S. Energy conversion of thermoacoustic engines with evaporation and condensation. Int J Heat Mass Transfer 2020;120385.
[21] Offner A, Yang R, Felman D, Elkayam N, Agnon Y, Ramon GZ. Acoustic oscillations driven by boundary mass exchange. J Fluid Mech 2019;866:316–49, ISSN 0022-1120, 1469-7645, 10.1017/jfm.2019.87.
[22] Swift GW. Thermoacoustics a unifying perspective for some engines and refrigerators. Acoust Soc Am 2003.
[23] Raspet R, Slaton WV, Hickey CJ, Hiller RA. Theory of inert gas-condensing vapor thermoacoustics: propagation equation. J Acoust Soc Am 2002;112(4):1414–22, ISSN 0001-4966. doi: 10.1121/1.1508113.
[24] Arnott WP, Bass HE, Raspet R. General formulation of thermoacoustics for stacks having arbitrarily shaped pore cross sections. J Acoust Soc Am 1991;90(6):3228–37.
[25] Swift GW, Garrett SL. Resonance reciprocity calibration of an ultracompliant transducer. J Acoust Soc Am 1987;81(5):1619–23, ISSN 0001-4966. doi: 10.1121/1.394514.
[26] Yang R, Meir A, Ramon GZ. Theoretical performance characteristics of a travelling-wave phase-change thermoacoustic engine for low-grade heat recovery. Appl Energy 2020;261:114377.
[27] Jin T, Yang R, Wang Y, Liu Y, Feng Y. Phase adjustment analysis and performance of a looped thermoacoustic prime mover with compliance/resistance tube. Appl Energy 2016;183:290–8.
[28] Belcher JR, Slaton WV, Raspet R, Bass HE, Lightfoot J. Working gases in thermoacoustic engines. J Acoust Soc Am 1999;105(5):2677–84.
[29] Tijani M, Zeegers J, De Waele A. Prandtl number and thermoacoustic refrigerators. J Acoust Soc Am 2002;112(1):134–43.
[30] Ordaz-Flores A, García-Valladares O, Gómez V. Findings to improve the performance of a two-phase flat plate solar system, using acetone and methanol as working fluids. Sol Energy 2012;86(4):1089–98.
[31] Pantaleo A, Simpson M, Rotolo G, Distaso E, Oyewunmi O, Sapin P, De Palma P, Markides C. Thermoeconomic optimisation of small-scale organic Rankine cycle systems based on screw vs. piston expander maps in waste heat recovery applications. Energy Conv Manage 2019;200:112053.
[32] Burkholder J, Hodnebrog O, Orkin V. Summary of abundances, lifetimes, ozone depletion potentials (ODPs), radiative efficiencies (REs), global warming potentials (GWPs), and global temperature change potentials (GTPs). Earth System Research Laboratories; 2018.
[33] Calm JM, Hourahan G. Refrigerant data update. HPAC Eng 2007;79(1):50–64.